Available online at www.sciencedirect.com

ScienceDirect

Ceramics International 40 (2014) 4697–4706

CERAMICS INTERNATIONAL

www.elsevier.com/locate/ceramint

A critical role of pH in the combustion synthesis of nano-sized $SrAl_2O_4$: Eu^{2+}, Dy^{3+} phosphor

Ehsan Shafia[a,*], Masoud Bodaghi[b], Serena Esposito[c], Alireza Aghaei[d]

[a]Department of Applied Science and Technology, Politecnico di Torino, Corso Duca degli Abruzzi 24, I-10129 Torino, Italy
[b]Engineering Design and Advanced Manufacturing, MIT Portugal Program, Faculty of Engineering, University of Porto, Porto, Portugal
[c]Department of Civil and Mechanical Engineering, Università degli Studi di Cassino e del Lazio Meridionale, Via G. Di Biasio 43, 03043 Cassino, FR, Italy
[d]Ceramic Department, Material and Energy Research Center (MERC), Karaj, Iran

Received 26 July 2013; received in revised form 30 July 2013; accepted 4 September 2013
Available online 21 September 2013

Abstract

Solution combustion synthesis of nano-crystalline $SrAl_2O_4$:Eu^{2+}, Dy^{3+} phosphor is investigated by varying the pH of the precursors solution, which plays an important role in phosphor's photoluminescence properties due to its ability to change the chemical environment of host structure surrounding Eu ions as an emission center. The best conditions for both intensity and decay behavior of the phosphor are achieved at pH of the precursors solution equal to 5.2, corresponding to the host structure composed of single-phase monoclinic $SrAl_2O_4$ without any impurity phases. Resulted phosphor shows a broad emission peak centered at 517 nm and excitation spectra consisting of two major peaks at 240 and 254 nm, well-known as characteristic peaks of this phosphor. Both the excitation and emission spectra of obtained nano-crystals shift to higher energies in contrast to the product of solid state method. These characteristic peaks are very weak or even absent in the samples resulted from precursors solution with higher or lower amount of pH than the "critical" pH. Crystallite size of the flake-shape particles is measured to be around 40 and 62 nm before and after thermal treatment, respectively.

Keywords: Combustion synthesis; pH; Nanostructures; Photoluminescence spectroscopy; $SrAl_2O_4$:Eu^{2+}, Dy^{3+}

1. Introduction

Long afterglow photoluminescence materials possess particular properties of storing light energy and glowing slowly in the dark environment. Compared to traditional sulfide-based phosphors, $SrAl_2O_4$-based phosphorescence materials are chemically stable and show excellent properties such as no radioactive radiation, and long and high-intensity afterglow and environmental compatibility. These materials have important applications in a variety of different industrial fields [1–4]. $SrAl_2O_4$:Eu^{2+}, Dy^{3+} phosphor shows a long period of luminescence after an initial rapid attenuation, and the lasting time of this kind of phosphors is more than 10 times than that of the previous sulfide phosphors [5,6].

An investigation of the mechanism of phosphorescence in $SrAl_2O_4$:Eu^{2+}, Dy^{3+} indicates that Eu^{2+} ions act as the emission centers and Dy^{3+} ions play a hole trap level role which is responsible for long lasting phosphorescence [7]. This long afterglow effect has been ascribed to the recombination between the trapped electrons at Eu^{2+} sites and thermally released holes trapped at Dy^{3+} sites, which strongly depends on the crystal structure of surrounding phase as host structure [8–12].

The compound $SrAl_2O_4$ as the host structure is formed by a three dimensional framework of corner-sharing AlO_4 tetrahedron. Each oxygen particle is shared by two aluminum ions so that each tetrahedron has one net negative charge that is balanced by the large divalent cations that occupy two different interstitial sites within the tetrahedral framework. It is worth mentioning that both of these two sites are nine fold coordinated. $SrAl_2O_4$ has two phases: a high-temperature hexagonal phase (HP) and a low-temperature monoclinic phase (MP). A reversible transition occurs at 650 °C [13–15].

*Corresponding author: Tel.: +39 011 564 4630; fax: +39 011 564 4699.
E-mail addresses: ehsan.shafia@polito.it (E. Shafia), masoud.bodaghi@fe.up.pt (M. Bodaghi), s.esposi@unicas.it (S. Esposito), a-aghaei@merc.ac.ir (A. Aghaei).

0272-8842/$ - see front matter © 2013 Elsevier Ltd and Techna Group S.r.l. All rights reserved.
http://dx.doi.org/10.1016/j.ceramint.2013.09.011

Many authors [16,17] reported the preparation of oxide based long-lasting phosphorescence materials of large size by using a solid-state reaction. In addition to the conventional problems of ceramic method, such as high temperature (in the case of $SrAl_2O_4$, above 1900 °C without flux, according to the phase diagram of $SrO–Al_2O_3$ system) [18] and formation of impurity phases due to the low homogeneity, the major drawback arises from product particle size. Fine particles can be obtained only by grinding the larger phosphor particles of solid-state reaction products, which can easily introduce more defects and greatly reduce the luminescence efficiency [16].

On account of developing new concepts for materials technology, different synthesis procedures for preparation of $SrAl_2O_4$ as the host structure and its phosphor have been set up based on the following methods: co-precipitation [1], sol–gel [18–22], reverse microemulsion [23], and combustion [24–37].

Among these techniques, the combustion method appears to be a more efficient technique for the synthesis of phosphors due to the relatively low reaction temperature and also high homogeneity and purity of the product due to good mixing of the starting materials at molecular level. Furthermore the combustion process is very facile, safe, instantaneous and energy saving and its products are essentially fine [24–37]. So far, the combustion synthesis procedure of $SrAl_2O_4:Eu^{2+}$, Dy^{3+} phosphor has been investigated by several authors [24–37]; nevertheless the role played by the pH of precursors solution on the host structure composition and afterglow characterizations still remains unexplored. The present paper describes the effect of precursors solution pH on the chemical composition of host structure and subsequently photoluminescence properties of final pigments.

2. Experimental

2.1. Materials

The purity and manufacturing of the chemicals used for the preparation of $SrAl_2O_4:Eu^{2+}$, Dy^{3+} phosphor are as follows: $Al(NO_3)_3 \cdot 09H_2O$ (99.9% pure), $Sr(NO_3)_2$ (99.9% pure), $Eu(NO_3)_3 \cdot 05H_2O$ (99.9% pure), $Dy(NO_3)_3 \cdot 05H_2O$ (99.9% pure) and urea ($CO(NH_2)_2$) as the fuel were provided from MERCK and used as received.

2.2. Powder synthesis

$Sr_{0.90}$ $Al_2O_4:Eu_{0.06}$, $Dy_{0.04}$ nano-crystalline phosphor was prepared via a solution combustion synthesis method followed by heating the precursor combustion ash at 1200 °C in reducing atmosphere. A stoichiometric mixture of $Al(NO_3)_3 \cdot 09H_2O$ and $Sr(NO_3)_2$ providing the host structure components and also Eu $(NO_3)_3 \cdot 05H_2O$ and $Dy(NO_3)_3 \cdot 05H_2O$, as a source of activator and co-activator ions, respectively, was dissolved in a minimum amount of distilled water together with 2.5 fold excess urea, as a preferred fuel for phosphor materials synthesis [37].

By slow heating at 75 °C and vigorous stirring for 5–6 h the precursors solution turned to a viscous gel. Adjustment of the solution pH is important to achieve high homogeneity in obtained gel. The resulted viscous gel was introduced into a muffle furnace with an air atmosphere and preheated at 600 °C. After a few seconds, the gel ignited spontaneously and underwent a very exothermic reaction, followed by decomposition with the evolution of large amounts of gases (oxides of carbon, nitrogen and ammonia). The whole process was over within less than 5 min and what remained was a voluminous and foamy combustion ash, which could be ground to very fine powder easily. This powder was subsequently annealed at 1200 °C in a weak reductive atmosphere ($5\%H_2+95\%N_2$) for 3 h to reduce the Eu^{3+} ions to Eu^{2+} as emission centers. Fig. 1 shows a flux diagram for the combustion synthesis method of $SrAl_2O_4:Eu^{2+}$, Dy^{3+} phosphor. More details about optimizing the synthesis process and phosphor composition have been reported in the previous issues [38–40].

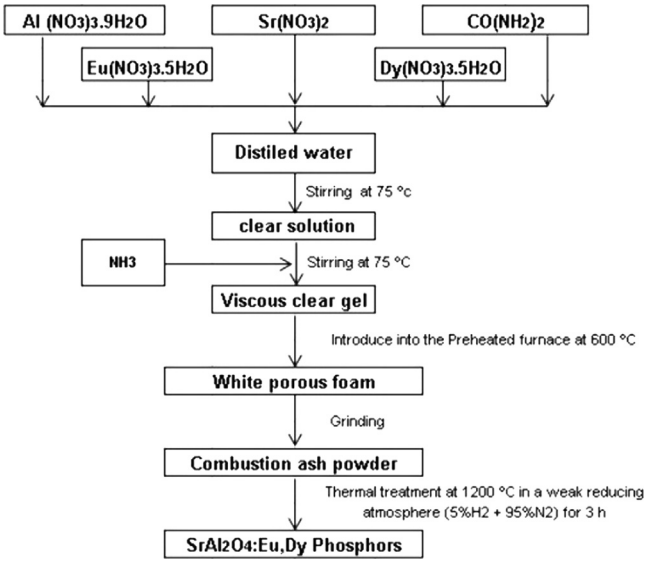

Fig. 1. Flux diagram for the combustion synthesis method of $SrAl_2O_4:Eu^{2+}$, Dy^{3+} phosphor.

2.3. Powder characterization

2.3.1. X-ray diffraction

XRD of the powders was carried out using a Siemens-Brucker D500 diffractometer, with voltage and current setting of 40 kV and 30 mA, respectively, and uses Cu Kα radiation (0.1541 nm). For quantitative and qualitative analysis, XRD diagrams were recorded in the interval $15^\circ \le 2\theta \le 45^\circ$ at a scan speed of 2°/min, giving a step size 0.02° and the step time 1 s. The average crystallite size of combustion ash powder and final phosphor was determined according to the broadening of main peaks of XRD patterns by means of Williamson–Hall plot and the Scherrer equation.

2.3.2. Photoluminescence spectroscopy

The luminescence properties of the obtained samples were measured at room temperature using a Perkin-Elmer LS-5

spectrometer. The luminescence intensity was measured over the wavelength 400–650 nm, while the excitation source was a xenon lamp (λ_{exc}=254 nm). The decay profiles were also recorded using the same instrument after the samples were excited for about 1 min by λ_{exc}=350 nm.

2.3.3. Scanning electron microscopy

The samples were coated with a thin layer of gold (Au) by sputtering (EMITECH K450X, England) and then the shape and morphology of prepared combustion ash foam and phosphors were observed on a scanning electron microscope (SEM; Philips XL 360) operated at the acceleration voltage of 20 kV.

2.3.4. Particle size distribution

The distribution of particle size of the final phosphor was checked by a Zetasizer 3000 HSA instrument.

3. Results and discussion

3.1. XRD analysis

Stoichiometric samples prepared by precursors solution at different pH show markedly different combustion behavior. pH equal to 2.3 leads to the white precipitation after a couple of hours heating and stirring due to the escape of water, which does not resolve by holding on heating, stirring and time. This sample does not show an ignition of combustion in the preheated furnace at 600 °C; it only boils and exhausts steams. The result of this process is a white hard crust. By contrast, transparent viscose gel without any precipitated materials is obtained at pH=5.2. This sample at the same initial temperature exhibits intense flame combustion with a large amount of exhausted gases and produces voluminous white foam covered by cracks and pours. This foam is easily converted to fine powder by mild grinding. At higher pH (pH=7.8), the final gel is semi-opalescent and shows weak combustion reaction in the preheated furnace and the resulted combustion foam is not as porous and smasher as the previous one.

As shown in Fig. 2, in the XRD pattern of the first sample (pH=2.3), the characteristic peaks of $SrAl_2O_4$ phase are very weak, while the $Sr_3Al_2O_6$ phase gives rise to the predominant peaks. $Sr_3Al_2O_6$ is an impurity phase, obtainable in an SrO–Al_2O_3 system at a considerably lower temperature than that of the $SrAl_2O_4$ phase.

In the present system, relatively lower adiabatic temperature of combustion reaction due to the incomplete ignition leads to the $Sr_3Al_2O_6$ phase formation [41]. The same phenomenon has been reported in the solid state synthesis of $SrAl_2O_4$:Eu^{2+}, Dy^{3+} phosphor with lower temperature as compared to the suitable temperature required for pure $SrAl_2O_4$ formation that leads to the $Sr_3Al_2O_6$ phase [2,3]. XRD patterns clearly indicate that, by increasing the pH of the solution to 5.2, a sample formed by the pure $SrAl_2O_4$ phase is obtained. On one hand, a complete ignition reaction provides enough energy to form the $SrAl_2O_4$ phase and on the other hand, high homogeneity obtained in the transparence viscous gel due to the absence of any preferential precipitation in precursors mixture eliminates the possibility of undesirable phases formation.

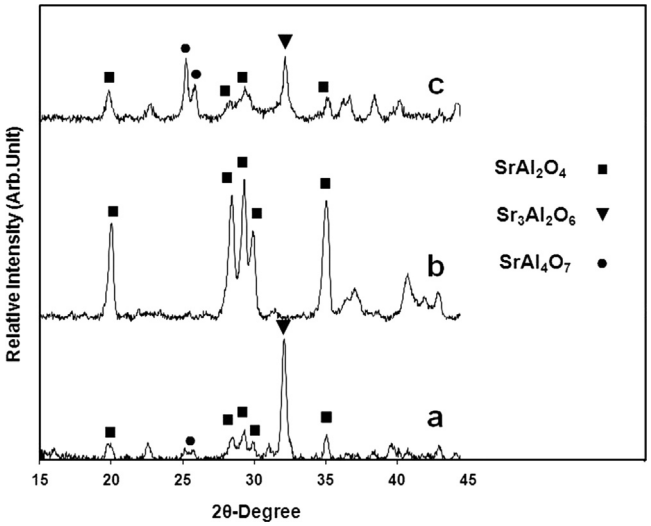

Fig. 2. XRD patterns of the combustion ash powder prepared by precursors solution of different pH: (a) pH=2.3, (b) pH=5.2 and (c) pH=7.8.

Pattern c, from the sample at pH=7.8, shows that the characteristic peaks of $SrAl_2O_4$ phase become weaker again and two impurity phases $Sr_3Al_2O_6$ and $SrAl_4O_7$ are observed. These phases are formed on account of preferential precipitate of aluminum oxohydroxide in the precursors solution.

Since the combustion synthesis is a method involving nucleation and growth mechanism, products are determined not only by the ignition conditions but also by the reactions occurring in the stock solution, where many processes take place simultaneously, affected by the type and concentration of metallic ions, present ligands and pH of solution.

In a real system according to the chemical conditions, aluminum ions undergo hydrolysis reactions to several different mononuclear hydroxides or polymerization reactions to polycations, which in dealing with the present ligands defines the final product [42,43]. Since formation of polynuclear hydrolysis products of aluminum is governed by the high reactivity of the $[Al(OH_2)_6]^{3+}$ ions in aqueous environment, this process is highly pH dependent [44].

As mentioned above, a more suitable chemical environment of the starting solution, to prevent preferential precipitation and obtain a good combustion reaction and the right phase composition after ignition, is obtained at the pH approximately around 5, corresponding to formation of an incorporated complex between metallic ions and urea, which is in fair agreement with Thomas et al.'s results, who proposed that in the pH range from 3.5 to 5 the predominant products of hydrolysis of Al ions in aqueous solution are dimeric or polymeric aluminum complexes [45]. The results of the ^{27}Al NMR studies of Bottero et al. validate this conclusion [46,47].

In the present case because of the poor coordinate bond forming ability of nitrate groups, they do not interfere in the reaction of hydroxide with the aluminum containing polymeric cation growing into bigger, charged polymeric species via olation and oxolation involving Al–OH–Al and Al–O–Al

bridges. But a point of interest is that water molecules might provide required bridging ligands and contribute to create an incorporated complex between metallic ions, hydroxyl groups and present ligands [48], which is associated with the elimination of preferential precipitation and warrants the homogeneity of precursors, demonstrated with transparency of obtained viscous gel and complete combustion reaction. By increasing pH, gelation occurs to an extent slightly greater than that corresponding to pH = 5.2. It is well known that in the neutral pH range ($5 < pH < 8$) aluminum trihydroxide (Al$(OH)_3$ (s)), also known as gibbsite and bayerite, starts to precipitate. Also, depending on time and conditions, aluminum trihydroxide can give one water molecule off to form pure boehmite (AlO(OH)) [45,47]. This evidence suggests that in the sample prepared with pH=7.8, preferential precipitation causes the lack of homogeneity and suitable complex formation. During the heterogeneous precipitation, little control over composition can be exercised due to the rapid changes in precursor material concentrations and localized discontinuous nature of the ligand introduction and consequent reaction. This separation in precursors would result in fast consumption of starting materials having undesirable compositions and subsequently prohibits the growth of main phase and also ignition combustion linked to the absence of complex between fuel and metallic ions.

At the same time we can say that pH=2.3 does not provide the right environment to form polynuclear complex [49] between metallic ions and urea, and so preferential precipitation occurred. Therefore pH = 5.2 of precursors solution is selected as critical pH. The *d*-spacing of crystal, relative diffraction strength (I/I_0) and index (*hkl*) of most intensive characteristic peaks of the sample with precursors solution pH adjusted at 5.2 are summarized in Table 1.

The contents of Table 1 indicate that pure $SrAl_2O_4$ phase in monoclinic form is achievable in the combustion step at the applied initial ignition temperature (600 °C), a considerably lower temperature as compared to the conventional solid-state reaction in which formation of pure $SrAl_2O_4$ phase is expected at >1350 °C with a flux (B_2O_3 or H_3BO_3) or at a higher temperature ignoring the flux [50,51]. The reason is attributed to the fact that the chemical energy released from the exothermic reaction between the nitrates species and fuel can rapidly heat the system to high temperatures (>1500 °C) during the combustion process and provide the desirable condition to form the pure $SrAl_2O_4$ phase [3]. It is worth noting that the high homogeneity of the components in solution is associated with formation of pure phase at relatively lower temperatures and meanwhile decreases the possibility of impurity phase formation.

Table 1
The crystal diffraction data: (*d*), (I/I_0) and (*hkl*) of the optimized sample with pH = 5.2 of precursors solution ignited at 600 °C.

I/I_0	2θ	*d* (nm)	*hkl*
100	29.10	3.066	220
88	28.23	3.158	211
86	34.88	2.570	211
71	29.77	2.999	211
67	19.82	4.470	101

In the binary SrO–Al_2O_3 system, several host phosphor compositions are known: $SrAl_2O_4$, $Sr_3Al_2O_6$ and $SrAl_4O_7$. Among these strontium aluminates, $SrAl_2O_4$ has got more phosphorescence efficiency when co-activated by Eu^{2+} and Dy^{3+}, with the emission peak around 520 nm [25]. Moreover in the case of $SrAl_2O_4$ according to references [50,51] and previous results obtained by this group [38,39], photoluminescence efficiency of $SrAl_2O_4$ in monoclinic shape is more than that in hexagonal shape. According to this fact, the best condition for phosphor afterglow (initial brightness and decay time) will be achieved in the presence of pure monoclinic $SrAl_2O_4$ which forms the surrounding environment of emission centers.

In general, afterglow originates from emission ions whose photo-excited electrons are thermally activated from traps. In $SrAl_2O_4$:Eu^{2+}, Dy^{3+} phosphor, the divalent Eu ions are excited to its 5d excited state under UV irradiation and play the role of emission center and Dy ions act as traps in the phosphorescence mechanism. Details of the phosphorescence mechanism and optimized content of activator (0.06) and co-activator (0.04) ions to obtain the best quality in phosphor afterglow have been reported in detail [38–40].

Reduction of Eu^{3+} to Eu^{2+}, which corresponds to the photoluminescence spectra in green region, was performed in a tube furnace with controllable atmosphere. Effect of thermal treatment step at 1200 °C in weak reducing atmosphere (5% H_2 + 95%N_2) for 3 h on the host structure and the appearance of synthesized phosphor are shown in Fig. 3.

XRD patterns show that there is no special change in the phase composition and purity of the host structure due to the applied thermal treatment on $SrAl_2O_4$ fine powder doped with activator and co-activator ions. It is observed that pure monoclinic $SrAl_2O_4$ is still the predominant phase in the annealed powders, without other product or starting materials; just relative increase in the peak intensity is due to the improvement in crystallization during the annealing step. Apart from this, the annealing step changes the color of particles from white in combustion ash powder to green in final phosphors (see Fig. 3, right) which is due to the change in Eu ions valences from 3+ to 2+ due to the larger stability of the latter Eu ions, reducing the Eu ions to 2+ by addition of an electron, and change in the electron configuration to $4f^7$. Green color could be related to the fact that Eu^{2+} ions absorb light energy equivalent to the difference in the energy levels of its f orbital.

In order to determine the crystallite size of both the combustion ash and final phosphor, the Williamson–Hall plot has been used as a useful tool for graphical demonstration of any *hkl*-dependence of broadening within a particular diffraction pattern. The instrumental line broadening of the measured profiles is corrected using ZrO_2 powder as the standard sample. The instrumental corrected broadening (β_{hkl}) corresponding to each diffraction peak was estimated from $\beta_{hkl} = [(\beta_{hkl})^2_{measured} - \beta^2_{instrumental}]^{0.5}$. In the Williamson–Hall method [52,53] it is assumed that the line

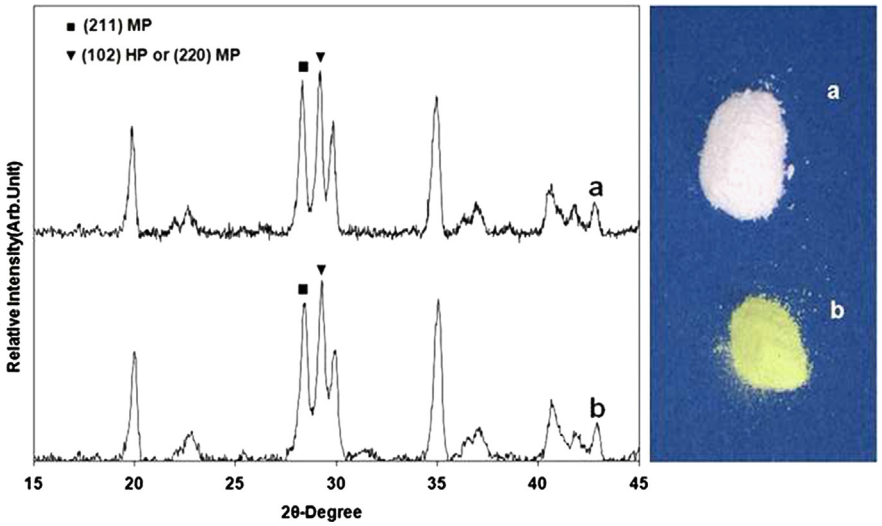

Fig. 3. Effect of thermal treatment at 1200 °C in weak reducing atmosphere ($5\%H_2+95\%N_2$) for 3 h on host structure of the sample with pH=5.2 of precursors solution: (left) XRD patterns and (right) appearance of synthesized powders—(a) combustion ash powder and (b) final pigment after thermal treatment. MP: Monoclinic phase, HP: Hexagonal phase of $SrAl_2O_4$.

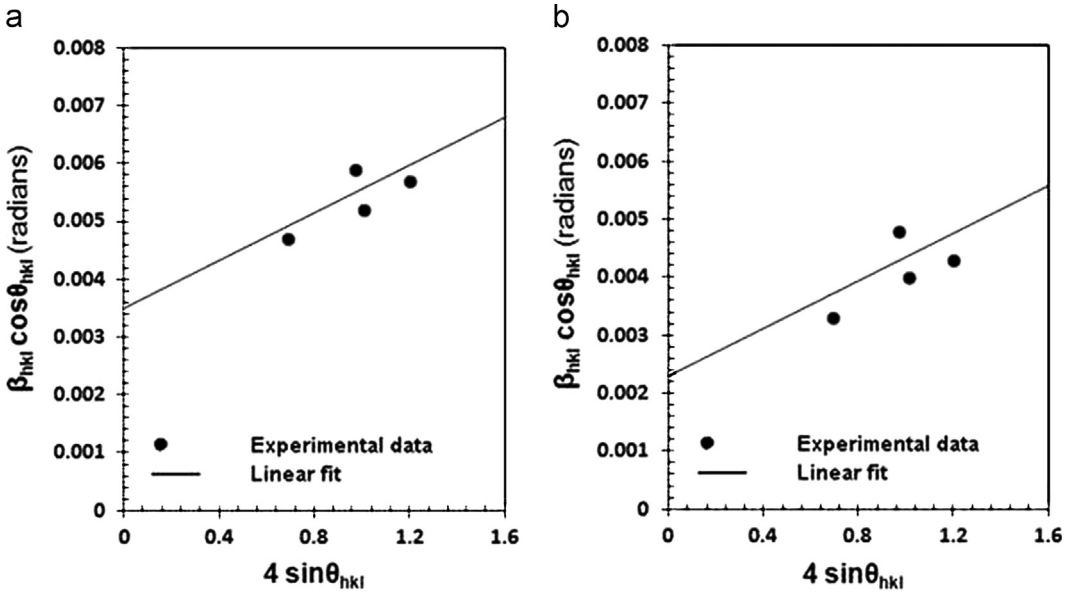

Fig. 4. Williamson–Hall plot of nanocrystals: (a) combustion ash and (b) phosphor.

broadening β_D of a Bragg reflection (*hkl*) originating from the small crystallite size follows the Scherrer equation $\beta_D=K\lambda/D\cos\theta_{hkl}$. Here K is the shape factor equal to 0.9, λ is the X-ray wavelength 0.1514 nm, θ_{hkl} is the Bragg angle and D is the effective crystallite size normal to the reflecting planes. Also, the strain induced broadening β_ε is given by the Wilson formula as $\beta\varepsilon=4\varepsilon\tan\theta_{hkl}$. Here ε is the root mean square value of the microstrain. Assuming that the particle size and strain contributions to line broadening are independent of each other and both have a Cauchy-like profile, the observed line breadth is simply the sum of the two i.e. $\beta_{hkl}=\beta D+\beta\varepsilon=[K\lambda/D\cos\theta_{hkl}]+[4\varepsilon\tan\theta_{hkl}]$ or $\beta_{hkl}\cos\theta_{hkl}=[K\lambda/D]+[4\varepsilon\sin\theta_{hkl}]$ which is the Williamson–Hall equation.

Plotting the value of $\beta_{hkl}\cos\theta_{hkl}$ as a function of $4\sin\theta_{hkl}$ the microstrain ε may be estimated from the slope of the line and the crystallite size from the intersection with the vertical axis. Fig. 4 shows the Williamson–Hall plot according to the patterns illustrated in Fig. 3. β_{hkl} values used here are the instrumentally corrected values and related to the peaks at $2\theta=19.82^\circ$, 28.23°, 29.10°, and 34.88°. Crystallite size of the particles is measured on average as 40 and 62 nm before and after thermal treatment, respectively [32,59], confirming crystal growth in the course of thermal treatment process.

3.2. Photo-physical analysis

3.2.1. Emission and excitation spectra

$SrAl_2O_4:Eu^{2+}$, Dy^{3+} phosphor is expected to be characterized by just one symmetrical broad-band emission spectrum centered at around 520 nm [38–40]. This emission band

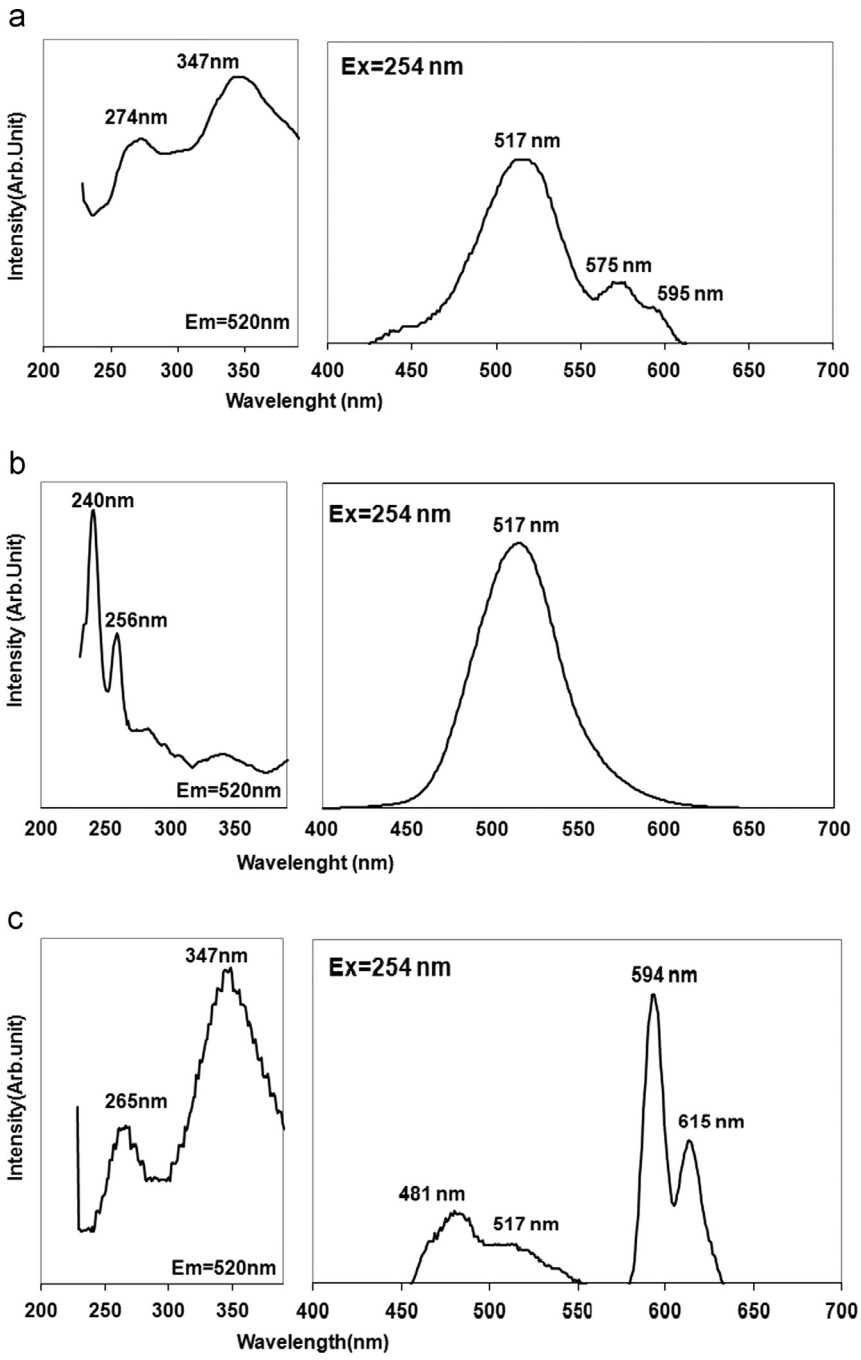

Fig. 5. Excitation (left) and emission (right) spectra of prepared phosphors with different pH of precursors solution: (a) pH=2.3, (b) pH=5.2 and (c) pH=7.8.

corresponds to the $4f^6 5d^1 \rightarrow 4f^7$ transition in Eu^{2+} ions; the 4f–5d transition in Eu^{2+} ions is an allowed one [28]. Excitation and emission spectra of the stoichiometric samples with different pH of precursors solution (2.3, 5.2 and 7.8) are compared in Fig. 5.

The symmetrical broad-band emission spectrum of $SrAl_2O_4$: Eu^{2+}, Dy^{3+} phosphor centered at 517 nm can be seen in the prepared sample with pH=5.2 of precursors solution (see Fig. 5b, right-hand graph) which is absent in the samples obtained at lower or higher pH than that of critical amount, in the presence of $Sr_3Al_2O_4$ and $SrAl_4O_7$ as impurity phases in the host structure (Fig. 5a and c, right-hand graphs).

In the case of $Sr_3Al_2O_4$ (Fig. 5a), the characteristic peak of phosphor at 517 nm is weaker in intensity and two unknown peaks at 575 and 595 nm (shoulder-like) are observable. In the same way, the spectrum of the sample with pH=7.8 shows that the characteristic peak of Eu^{2+} emission centers in $SrAl_2O_4$ phase become weaker and three new peaks with different intensities are observed. The predominant peak centered at 595 nm is the same with sample pH=2.3 but with more intensity (Fig. 5c). These phenomena could be related to the different chemical environments surrounding emission centers and changed electron configuration of Eu ions. It is well known that emission of Eu^{2+} ions as an emission center

in $SrAl_2O_4:Eu^{2+}$ phosphors very strongly depends on the host lattice structure and can occur from the ultraviolet to the red region with a variety of initial intensity. Consequently, excited $4f^65d^1$ configurations of Eu^{2+} ions are extremely sensitive to the change in the lattice environment. In contrast to the electrons in the inner shell, the 5d electron may couple strongly to the lattice [50–61].

These results confirm that the efficiency of $SrAl_2O_4$ phase for photoluminescence emission around 520 nm is more than those of two other phases. Comparable results were reported by Akiyama et al. about the phosphorescence efficiency of $SrAl_2O_4$, $Sr_3Al_2O_6$, and $SrAl_4O_7$ phases as the host structure for Eu emission centers [25].

The same condition could be shown in the excitation spectra of these samples. As illustrated in Fig. 5a–c (left-hand graphs) change in the chemical composition of the host structure gives rise to the loss of known excitation peaks at 240 and 256 nm for $SrAl_2O_4:Eu^{2+}$, Dy^{3+} phosphor, due to the changed chemical environment and electron configuration of Eu ions.

The luminescence properties of $SrAl_2O_4:Eu^{2+}$, Dy^{3+} prepared by the solid-state method have been studied by other authors [15–17,59]. In $SrAl_2O_4:Eu^{2+}$ phosphor, Eu^{2+} ions showed two broad emission bands at about 445 and 520 nm at 4.2 K, which were due to the substitution of Eu^{2+} ions for Sr^{2+} ions in two different lattices. But the luminescence spectrum of Eu^{2+} is also more sensitive to temperature quenching. Therefore, at room temperature, the emission at 445 nm is almost quenched and only the longer wavelength emission at 520 nm is observed [59].

By comparing the spectral characters of phosphors prepared by the combustion method and conventional solid state reaction, it is easy to notice that the emission and excitation bands show a slight blue-shift in combustion products. In our case, the emission band lies at about 517 nm. The electric dipole-allowed transition, $4f^7$–$4f^65d^1$, originating from bivalent europium doped strontium aluminate seems to have profound dependence on the particle size. Because the 5d energy level has close relation to the conduction band, when the grain size becomes small, the band gap may become wide or narrow; then the 5d energy level also changes correspondingly. So, it should be also noted that the position of the emission band in nano-crystals shifts to higher energies in contrast to the bulk materials obtained from the solid state reaction [59].

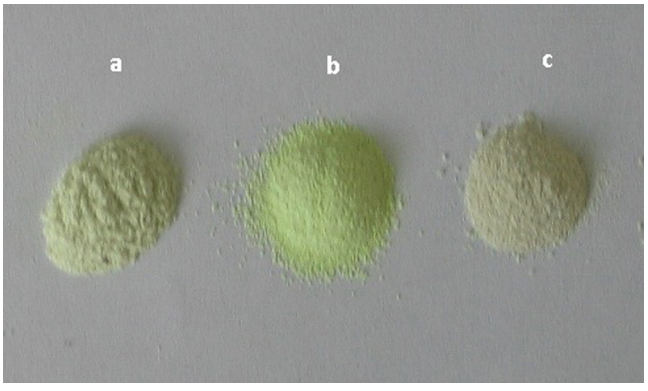

Fig. 6. Effect of different pH of precursors solution on the appearance color of final pigments: (a) pH=2.3, (b) pH=5.2 and (c) pH=7.8.

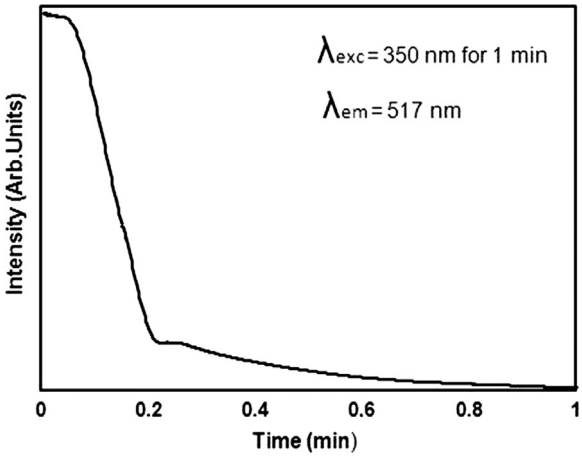

Fig. 7. The decay time curve of $SrAl_2O_4:Eu^{2+}$, Dy^{3+} phosphors prepared with pH=5.2 precursors solution resulting from deoxidization stage, $\lambda_{exc}=350$ nm and $\lambda_{em}=517$ nm.

Interestingly, changing the pH of precursors solution introduces profound difference in the color of synthesized phosphors. Fig. 6 depicts the final synthesized phosphors with different pH of precursors solution (2.3, 5.2 and 7.8) after thermal treatment in reductive atmosphere. The gray color could be due to the uncompleted ignition and arising from organic residue in the products especially in the sample with pH=7.8.

3.2.2. Decay curves and afterglow characteristics

The decay time curve of $SrAl_2O_4:Eu^{2+}$, Dy^{3+} phosphors resulting from a deoxidization stage (final pigments) of the sample synthesized with pH=5.2 of precursor solution is shown in Fig. 7. The result indicates that the decay process contained a rapid-decay process and a slow-decay process. The decay rate is very large before 0.2 min after removing the excitation source immediately. The afterglow intensity gradually became constant after this time [61,62]. The samples with pH=2.3 and 7.8 do not show any decay time curve under excitation λ_{exc}=350 nm for expected emission at λ_{em}=517 nm. The shallow traps for holes and Sr^{2+} vacancies in the host structure introduced by Dy^{3+} ions are responsible for the rapid-decay process, as the shallow traps release the holes to the recombination process, after cutting off the excitation source immediately. On the other hand, the Sr^{2+} vacancy transmits the excitation energy to emission centers. Finally, the cation vacancy has a large effect on the phosphorescence mechanism in alkaline earth aluminates phosphors [63,64]. According to the literature the fluorescence lifetime of nanocrystal is shorter than that of bulk crystal, the decrease in the lifetime when the particle size is decreased seems possible, and maybe due to nonradiation relaxation caused by surface defects and hydrated or carbonated species that act as quenching centers [59].

Photoluminescence emission of the above-mentioned sample after excitation by 350 nm radiation for 1 min in the dark room is depicted in Fig. 8.

3.3. SEM observations

The microstructure of the combustion ash foams and $SrAl_2O_4:Eu^{2+}$, Dy^{3+} phosphor fine particles is evaluated by scanning electron microscopy (see Fig. 9). As mentioned above the resulted foam of the combustion has a very smasher and brittle structure. In all samples the surfaces of combustion ash foams have a lot of cracks, voids and pores due to released gases during the combustion reaction (Fig. 9a–c).

These features are more significant in the sample with pH = 5.2 due to the high degree of ignition and complete combustion in preheated kiln where more exothermic reactions cause higher temperature and more volume of released gases. The final pigments show a very thin flake shape (Fig. 9d) in the relatively wide range of size distribution.

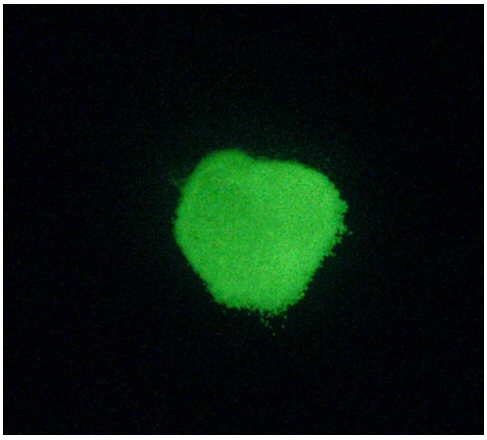

Fig. 8. Emission of pigment synthesized with pH = 5.2 precursors solution after excitation by 350 nm radiation for 1 min in the dark room.

3.4. Particle size distribution

Size distribution of final phosphor particles after thermal treatment from the sample prepared by pH = 5.2 of precursors solution was checked by the Zetasizer instrument as shown in Fig. 10.

A wide range of particles distribution that starts from below 35 nm with two maximums at around 300 nm and more than 1 μm with the most particles detected in the range of 75–1000 nm is observable. According to our hypotheses, the particles synthesized by the same conditions cannot have very different sizes in this scale; hence, this variation could be rationalized by special flake shape of the particles and random orientation of detection in the instrument; these facts are supported by SEM observations. Variation in particle size might also result from the agglomeration of very fine particles synthesized by the combustion process. As observed from the experiments, nanoparticles were made within the first few minutes, and then the particles got aggregated because of their large surface area to volume ratio. Due to increase in the surface area to the volume ratio, the attractive force between

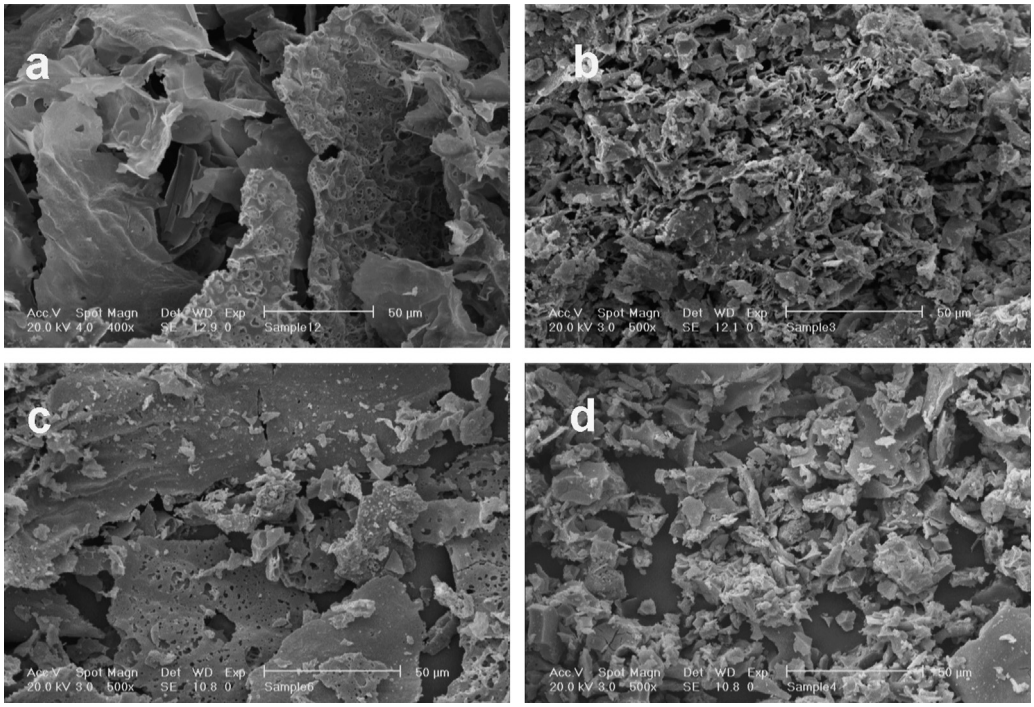

Fig. 9. Scanning electron microscopy images of combustion ash foam related to the samples with precursors solution pH of (a) 2.3, (b) 5.2 and (c) 7.8. (d) Final particle resulted from thermal treatment.

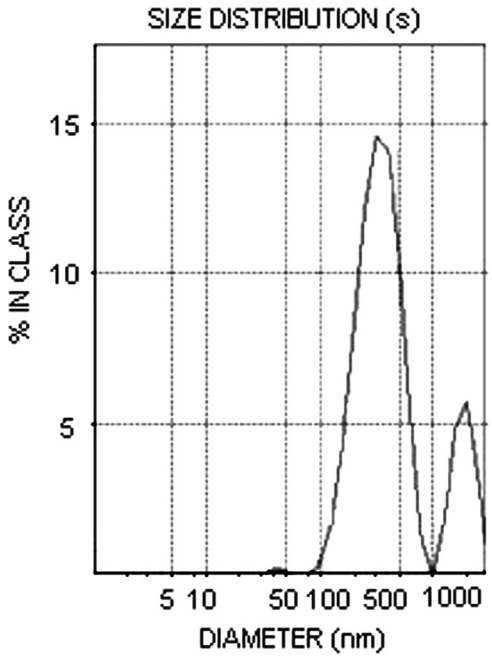

Fig. 10. Size distribution of final phosphor particles evaluated by Zetasizer instrument after thermal treatment step at 1200 °C in weak reducing atmosphere (5%H_2+95%N_2) for 3 h, sample prepared with precursors solution of pH=5.2.

the nanoparticles increased, which leads to the agglomeration of the particles.

4. Conclusion

The effect of different pH of precursors solution in combustion synthesis of $SrAl_2O_4$:Eu^{2+}, Dy^{3+} phosphor has been investigated. The single phase of monoclinic $SrAl_2O_4$ as the host structure is obtainable by heating the transparent gel precursor for a few minutes at 600 °C, a markedly lower temperature as compared to conventional solid-state reaction. The experimental results strongly indicate that pH of the precursor solution is a key factor in the combustion synthesis of nano-sized $SrAl_2O_4$:Eu^{2+}, Dy^{3+} phosphor, as it influences the development of the combustion reaction, the chemical composition of host structure and spectroscopic feature of phosphors. $SrAl_2O_4$:Eu^{2+}, Dy^{3+} phosphor with the best afterglow quality can be obtained at critical pH of the precursors solution equal to 5.2. This critical pH value is affected by the hydrolysis process and polymerization reactions of the selected metal nitrates and especially urea content. Results indicate that the effect of precursors solution pH on the afterglow characterization is directly related to the change in the chemical structure surrounding the Eu ions as an emission center. It is revealed that among the three aluminates $SrAl_2O_4$, $Sr_3Al_2O_6$ and $SrAl_4O_7$ from the SrO–Al_2O_3 binary system, $SrAl_2O_4$ has got more phosphorescence efficiency as the host structure for Eu ions for emission in the green region. Final pigments show a very thin flake shape and calculated crystalline sizes are 40 and 62 nm, for combustion ash powder and final pigments, respectively.

References

[1] Y. Lin, Z. Zhang, F. Zhang, Z. Tang, Q. Chen, Preparation of the ultrafine $SrAl_2O_4$: Eu, Dy needle-like phosphor and its optical properties, Materials, Chemistry and Physics 65 (2000) 103–106.
[2] X. Fu, H. Yamada, C.N. Xu, Property of highly oriented $SrAl_2O_4$:Eu film on quartz glass substrates and its potential application in stress sensor, Journal of the Electrochemical Society 156 (2009) J249–J252.
[3] T. Peng, H. Yang, X. Pu, B. Hu, Z. Jiang, C. Yan, Combustion synthesis and photoluminescence of $SrAl_2O_4$:Eu,Dy phosphor nanoparticles, Materials Letters 58 (2004) 352–356.
[4] R. Chen, Y. Wang, Y. Hu, Z. Hu, C. Liu, Modification on luminescent properties of $SrAl_2O_4$:Eu^{2+},Dy^{3+} phosphor by Yb^{3+} ions doping, Journal of Luminescence. 128 (2008) 1180–1184.
[5] Y. Liu, B. Lei, C. Shi, Luminescent properties of a white afterglow phosphor $CdSiO_3$:Dy^{3+}, Chemistry of Materials 17 (2005) 2108–2113.
[6] E. Nakazawa, T. Mochida, Traps in $SrAl_2O_4$:Eu^{2+} phosphor with rare-earth ion doping, Journal of Luminescence 72 (1997) 236–237.
[7] D. Haranath, V. Shanker, H. Chander, P. Sharma, Studies on the decay characteristics of strontium aluminate phosphor on thermal treatment, Materials Chemistry and Physics 78 (2002) 6–10.
[8] M.D. Segall, P.L.D. Lindan, M.J. Probert, C.J. Pickard, P.J. Hasnip, S. J. Clark, M.C. Payne, First-principles simulation: ideas, illustrations and the CASTEP code, Journal of Physics: Condensed Matter 14 (2002) 2717–2744.
[9] J.P. Perdew, S. Burke, M. Ernzerhof, Generalized gradient approximation made simple, Physical Review Letters 77 (1996) 3865–3868.
[10] T. Aitasalo, J. Holsa, H. Jungner, M. Lastusaari, J. Niittykoski, Sol–gel processed Eu^{2+}-doped alkaline earth aluminates, Journal of Alloys and Compounds 341 (2002) 76–78.
[11] Y.H. Lin, Z.T. Zhang, F. Zhang, Z.L. Tang, Q.M. Chen, Preparation of the ultrafine $SrAl_2O_4$: Eu, Dy needle-like phosphor and its optical properties, Materials Chemistry and Physics 65 (2000) 103–106.
[12] W. Jia, H. Yuan, L. Lu, H. Liu, W.M. Yen, Phosphorescent dynamics in $SrAl_2O_4$: Eu^{2+}, Dy^{3+} single crystal fibers, Journal of Luminescence 76 (1998) 424–428.
[13] A. Nag, T.R.N. Kutty, Role of B_2O_3 on the phase stability and long phosphorescence of $SrAl_2O_4$: Eu, Dy, Journal of Alloys and Compounds 354 (2003) 221–231.
[14] W.S. Shi, H. Yamada, K. Nishikubo, H. Kusaba, C.N. Xu, Novel structural behavior of strontium aluminate doped with europium, Journal of the Electrochemical Society 151 (2004) H97–H100.
[15] Y. Lin, Z. Zhang, Z. Tang, J. Zhang, Z. Zheng, X. Lu, The characterization and mechanism of long afterglow in alkaline earth aluminates phosphors co-doped by Eu_2O_3 and Dy_2O_3, Materials Chemistry and Physics 70 (2001) 156–159.
[16] R.P. Rao, Preparation and characterization of fine-grain yttrium-based phosphors by sol–gel process, Journal of the Electrochemical Society 143 (1996) 189–197.
[17] T. Matsuzawa, Y. Aoki, N. Takeuchi, Y. Murayama, A new long phosphorescent phosphor with high brightness, $SrAl_2O_4$: Eu^{2+}, Dy^{3+}, Journal of the Electrochemical Society 143 (1996) 2670–2673.
[18] P. Escribano, M. Marchal, M.L. Sanjuán, P. Alonso-Gutiérrez, B. Julián, E. Cordoncillo, Low-temperature synthesis of $SrAl_2O_4$ by a modified sol–gel route: XRD and Raman characterization, Journal of Solid State Chemistry 178 (2005) 1978–1987.
[19] X. Liyuan, X. Qin, L. Yingliang, Preparation and characterization of flower-like $SrAl_2O_4$:Eu^{2+}, Dy^{3+} phosphors by sol–gel process, Journal of Rare Earths 29 (2011) 39–43.
[20] L.K. Kurihara, S.L. Suib, Sol–gel synthesis of ternary metal oxides.1. Synthesis and characterization of MAl_2O_4 (M=Mg, Ni, Co, Cu, Fe, Zn, Mn, Cd, Ca, Hg, Sr, and Ba) and lead aluminum oxide ($Pb_2Al_2O_5$), Chemistry of Materials 5 (1993) 609–613.
[21] T. Peng, L. Huajun, H. Yang, C. Yan, Synthesis of $SrAl_2O_4$: Eu, Dy phosphor nanometer powders by sol–gel processes and its optical properties, Materials Chemistry and Physics 85 (2004) 68–72.
[22] Y Wu, Y Wang, D He, M Fu, Y Zhao, Y Li, F Miao, Synthesis and luminescence properties of Sr_2SiO_4:Eu^{3+}, Dy^{3+} phosphors by the

sol–gel method, Journal of Nanoscience and Nanotechnology 11 (2011) 9439–9444.
[23] C.H. Lu, S.Y. Chen, C.H. Hsu, Nanosized strontium aluminate phosphors prepared via a reverse microemulsion route, Journal of Materials Science and Engineering B 140 (2007) 218–221.
[24] Y. Zhang, Z. Chen, Z. Zhou, Rapid combustion synthesis of light-storing–emitting material $SrAl_2O_4:Eu^{2+}\cdot Dy^{3+}$ and its spectral characteristics, Journal of Electrochemical Society 153 (2006) H86–H87.
[25] M. Akiyama, C.N. Xu, Y. Liu, K. Nonaka, T. Watanabe, Influence of Eu, Dy co-doped strontium aluminate composition on mechanoluminescence intensity, Journal of Luminescence 97 (2002) 13–18.
[26] J.J. Kingsley, K. Suersh, K.C. Patil, Combustion synthesis of fine-particle metal aluminates, Journal of Materials Science 25 (1990) 1305–1312.
[27] Z. Fu, S. Zhou, S. Zhang, Study on optical properties of rare-earth ions in nanocrystalline monoclinic $SrAl_2O_4$: Ln ($Ln=Ce^{3+}$, Pr^{3+}, Tb^{3+}), Journal of Physical Chemistry B 109 (2005) 14396–14400.
[28] Y.P. Fu, Preparation of $Y_3Al_5O_{12}$: Eu powders by microwave-induced combustion process and their luminescent properties, Journal of Alloys and Compounds 402 (2005) 233–236.
[29] J. Dhanaraj, R. Jagannathan, T.R.N. Kutty, C.H Lu, Study on optical properties of rare-earth ions in nanocrystalline monoclinic $SrAl_2O_4$: Ln ($Ln=Ce^{3+}$, Pr^{3+}, Tb^{3+}), Journal of Physical Chemistry B 105 (2001) 11098–11105.
[30] S.K Shi, J.Y Wang, Combustion synthesis of Eu^{3+} activated $Y_3Al_5O_{12}$ phosphor nanoparticles, Journal of Alloys and Compounds 327 (2001) 82–86.
[31] R. Zhang, G. Han, L. Zhang, B. Yang, Gel combustion synthesis and luminescence properties of nanoparticles of monoclinic $SrAl_2O_4:Eu^{2+}$, Dy^{3+}, Materials Chemistry and Physics 113 (2009) 255–259.
[32] N.M. Son, L.T.T. Vien, L.V.K. Bao, N.N. Trac, Synthesis of $SrAl_2O_4$: Eu^{2+} Dy^{3+} phosphorescence nanosized powder by combustion method and its optical properties, Journal of Physics: Conference Series 187 (2009) 012017.
[33] X. Yu, C. Zhou, X. He, Z. Peng, S. Yang, The influence of some processing conditions on luminescence of $SrAl_2O_4:Eu^{2+}$ nanoparticles produced by combustion method, Materials Letters 58 (2004) 1087–1091.
[34] K.C. Patil, S.T. Aruna, T. Mimani, Combustion synthesis: an update, Current Opinion in Solid State & Materials Science 6 (2002) 507–512.
[35] H. Chander, D. Haranath, V. Shanker, P. Sharma, Synthesis of nanocrystals of long persisting phosphor by modified combustion technique, Journal of Crystal Growth 271 (2004) 307–312.
[36] T Mimani, K.C Patil, Solution combustion synthesis of nanoscale oxides and their composites, Materials Physics and Mechanics 4 (2001) 134–137.
[37] S.T. Aruna, A.S. Mukasyan, Luminescent and structural properties of $MgNb_2O_6$ nanocrystals, Current Opinion in Solid State & Materials Science 12 (2008) 44–50.
[38] E. Shafia, M. Bodaghi, M. Tahriri, The influence of some processing conditions on host crystal structure and phosphorescence properties of $SrAl_2O_4:Eu^{2+}$, Dy^{3+} nanoparticle pigments synthesized by combustion technique, Current Applied Physics 10 (2010) 596–600.
[39] E. Shafia, A. Aghaei, M. Bodaghi, M. Tahriri, Combustion synthesis, structural and photo-physical characteristics of Eu^{2+} and Dy^{3+} co-doped $SrAl_2O_4$ phosphor nanopowders, Journal of Materials Science: Materials in Electronics 22 (2011) 1136–1142.
[40] E. Shafia, A. Aghaei, A. Davarpanah, M. Bodaghi, M. Tahriri, S. H. Alavi, Synthesis and characterization of $SrAl_2O_4:Eu^{2+}$, Dy^{3+} nanocrystalline phosphorescent pigments, Transactions of the Indian Ceramic Society 70 (2011) 71–77.
[41] W. Minquan, D. Wang, L. Guanglie, Research on fluorescence spectra and structure of single-phase $4SrO\cdot 7Al_2O_3:Eu^{2+}$ phosphor prepared by solid-state reaction method, Materials Science and Engineering B 60 (1998) 18–23.
[42] A.W. Thomas, A.P. Tai, The nature of aluminum oxide hydrosols, Journal of the American Chemical Society 54 (1932) 841–855.
[43] T. Ikeda, M. Hirata, T. Kimura, Hydrolysis of Al^{3+} from constrained molecular dynamics, Journal of Chemical Physics 124 (2006) 074503.
[44] J.W. Akitt, N.N. Greenwood, B.L. Khandelwal, G.D. Lester, ^{27}Al nuclear magnetic resonance studies of the hydrolysis and polymerisation of the hexa-aquo-aluminium (III) cation, Journal of the Chemical Society A 5 (1972) 604–610.
[45] F. Thomas, A. Masion, J.Y. Bottero, J. Rouiller, F. Genévrier, D. Boudot, Aluminum (III) speciation with acetate and oxalate. A potentiometric and aluminum-27 NMR study, Environmental Science and Technology 25 (1991) 1553–1559.
[46] J.Y. Bottero, J.M. Cases, F. Fiessinger, J.E. Poirier, Studies of hydrolyzed aluminum chloride solutions. 1. Nature of aluminum species and composition of aqueous solutions, Journal of Physical Chemistry 84 (1980) 2933–2939.
[47] J.Y. Bottero, M. Axelos, D. Tchoubar, J.M. Cases, J.J. Fripiat, F. Fiessinger, Mechanism of formation of aluminum trihydroxide from keggin Al_{13} polymers, Journal of Colloid and Interface Science 117 (1987) 47–57.
[48] S. Ramanathan, S.K. Roy, R. Bhat, D.D. Upadhyaya, A.R. Biswa, Alumina powders from aluminium nitrate–urea and aluminium sulphate–urea reactions — the role of the precursor anion and process conditions on characteristics, Ceramic International 23 (1997) 45–53.
[49] C. Brosset, On the reactions of the aluminium ion with water, Acta Chemica Scandinavica 6 (1952) 910–940.
[50] Y. Lin, Z. Zhang, Z. Tang, J. Zhang, Z. Zheng, X. Lu, The characterization and mechanism of long afterglow in alkaline earth aluminates phosphors co-doped by Eu_2O_3 and Dy_2O_3, Materials Chemistry and Physics 70 (2001) 156–159.
[51] J. Sanchez-Benitez, A. de Andres, M. Marchal, E. Cordoncillo, M. Vallet Regi, P. Escribano, Optical study of $SrAl_{1.7}B_{0.3}O_4$:Eu, R (R=Nd, Dy) pigments with long-lasting phosphorescence for industrial uses, Journal of Solid State Chemistry 171 (2003) 273–277.
[52] G.K. Williamson, W.H. Hall, X-ray line broadening from filed aluminium and wolfram, Acta Metallurgica 1 (1953) 22–31.
[53] H.P. Klug, L.E. Alexander, X-Ray Diffraction Procedures: For Polycrystalline and Amorphous Materials, 2nd ed., Wiley, 1974.
[54] A. Nag, T.R.N. Kutty, The mechanism of long phosphorescence of $SrAl_{2-x}B_xO_4$ ($0<x<0.2$) and $Sr_4Al_{14-x}B_xO_{25}$ ($0.1<x<0.4$) co-doped with Eu^{2+} and Dy^{3+}, Materials Research Bulletin 39 (2004) 331–342.
[55] S.H.M. Poort, W.P. Blokpoel, G. Blasse, Luminescence of Eu^{2+} in barium and strontium aluminate and gallate, Journal of Chemistry and Materials 7 (1995) 1547–1551.
[56] D. Ravichandran, S.T. Johnson, S. Erdei, R. Roy, W.B. White, Crystal chemistry and luminescence of the Eu^{2+}-activated alkaline earth aluminate phosphors, Displays 19 (1999) 197–203.
[57] Z.C. Wu, J.X. Shi, J. Wang, H. Wu, Q. Su, M.L. Gong, Synthesis and luminescent properties of $SrAl_2O_4:Eu^{2+}$ green-emitting phosphor for white LEDs, Materials Letters 60 (2006) 3499–3501.
[58] K.V.d. Eeckhout, P.F. Smet, D. Poelman, Persistent luminescence in Eu^{2+}-doped compounds: a review, Journal of Materials 3 (2010) 2536–2566.
[59] Z.L. Fu, S.H. Zhou, Y.N Yu, S.Y. Zhang, Combustion synthesis and luminescence properties of nanocrystalline monoclinic $SrAl_2O_4:Eu^{2+}$, Chemical Physics Letters 395 (2004) 285–289.
[60] H. Ryu, K.S. Bartwal, Defect structure and its relevance to photoluminescence in $SrAl_2O_4:Eu^{2+}$, Nd^{3+}, Physica B 404 (2009) 1714–1718.
[61] J. Holsa, H. Jungner, M. Lastusaari, J. Niittykoski, Persistent luminescence of Eu^{2+} doped alkaline earth aluminates, $MAl_2O_4:Eu^{2+}$, Journal of Alloys and Compounds 326 (2001) 326–330.
[62] Y. Lu, Y. Li, Y. Xiong, D. Wang, Q. Yin, $SrAl_2O_4$: Eu^{2+}, Dy^{3+} phosphors derived from a new sol–gel route, Journal of Microelectronics 35 (2004) 379–382.
[63] A.J. Lenus, K.G. Rajan, M. Yousuf, D. Sornadurai, B. Purniah, Luminescence behaviour of rare earth doped alkaline earth aluminates prepared by the halide route, Materials Letters 54 (2002) 70–74.
[64] T. Aitasalo, P. Deren, J. Holsa, H. Jungner, J.C. Krupa, M. Lastusaari, J. Legendziewicz, J. Niittykoski, W. Strek, Persistent luminescence phenomena in materials doped with rare earth ions, Journal of Solid State Chemistry 171 (2003) 114–121.